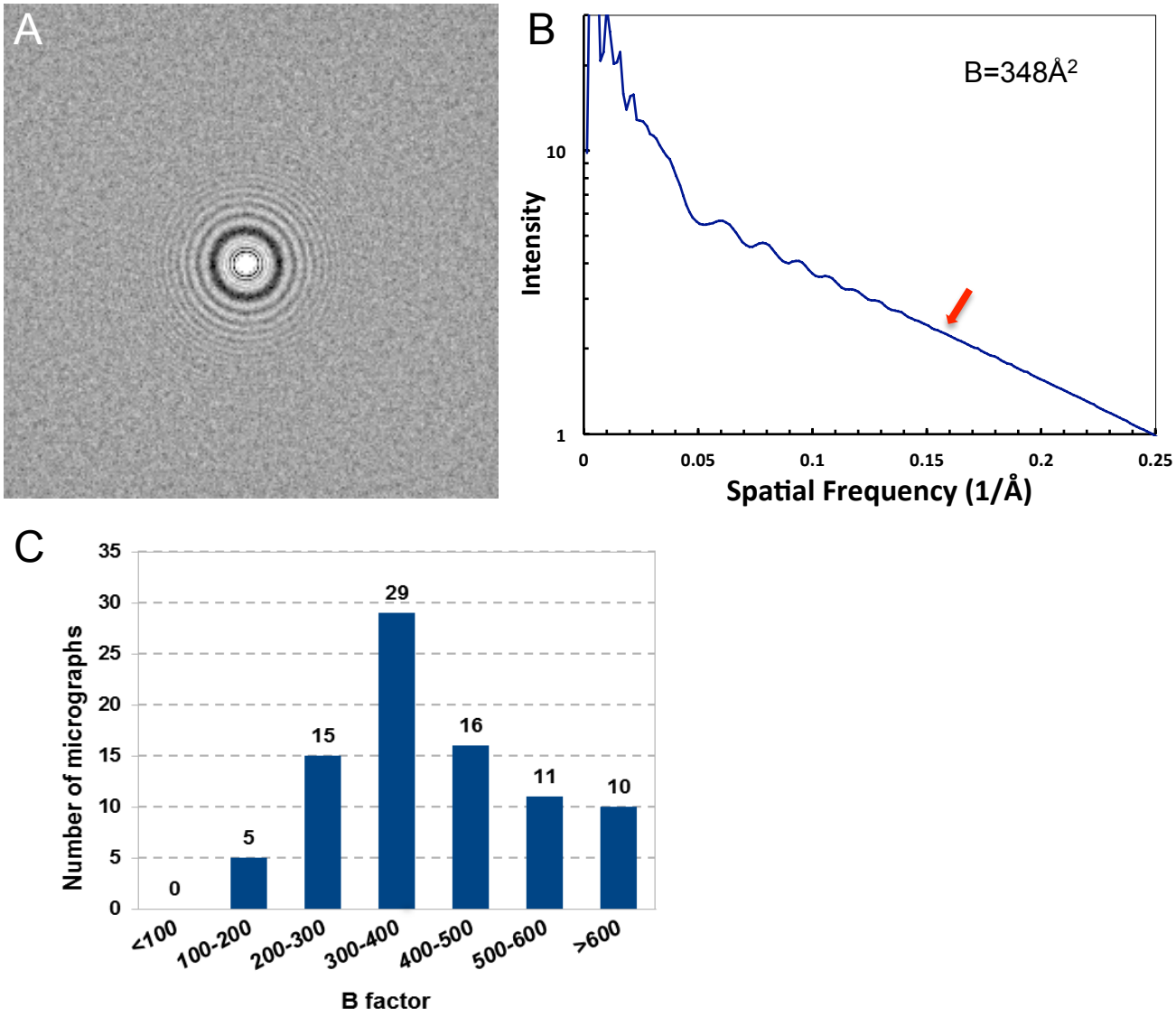

Figure S1. Related to Figure 1. Cryo-EM image quality assessment. Shown are 2-D (A) and 1-D (B) power spectra of the micrograph shown in Figure 1A. The defocus and B-factor of this micrograph is 1.98 μm and 348 Å^2, respectively. The highest resolution visible Thon ring (marked by red arrow in (B) is at about 6.8 Å. (C) The B-factor distribution of all 86 micrographs.

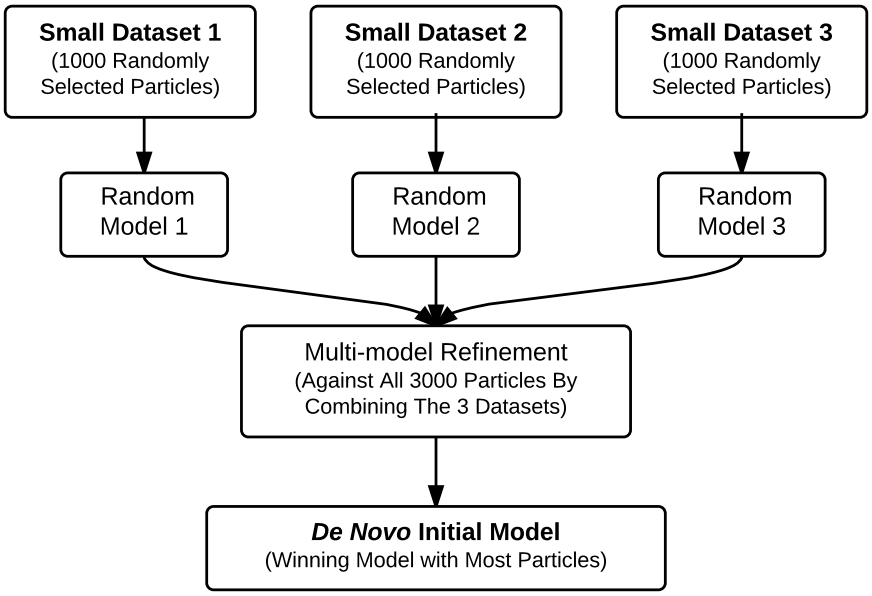

Figure S2. Related to Figures 2 and 3. Flowchart of *de novo* initial model determination method. This figure shows expanded details for the **De Novo Initial Model** boxes in Figure 2. The typical *de novo* random model approach (represented by the three **Random Model** boxes in this figure) was enhanced with further competitive multi-model refinement (represented by the **Multi-model Refinement** box) to more reliably reach correct initial model for challenging datasets such as the close-packed PCV2 particles with smooth surfaces.

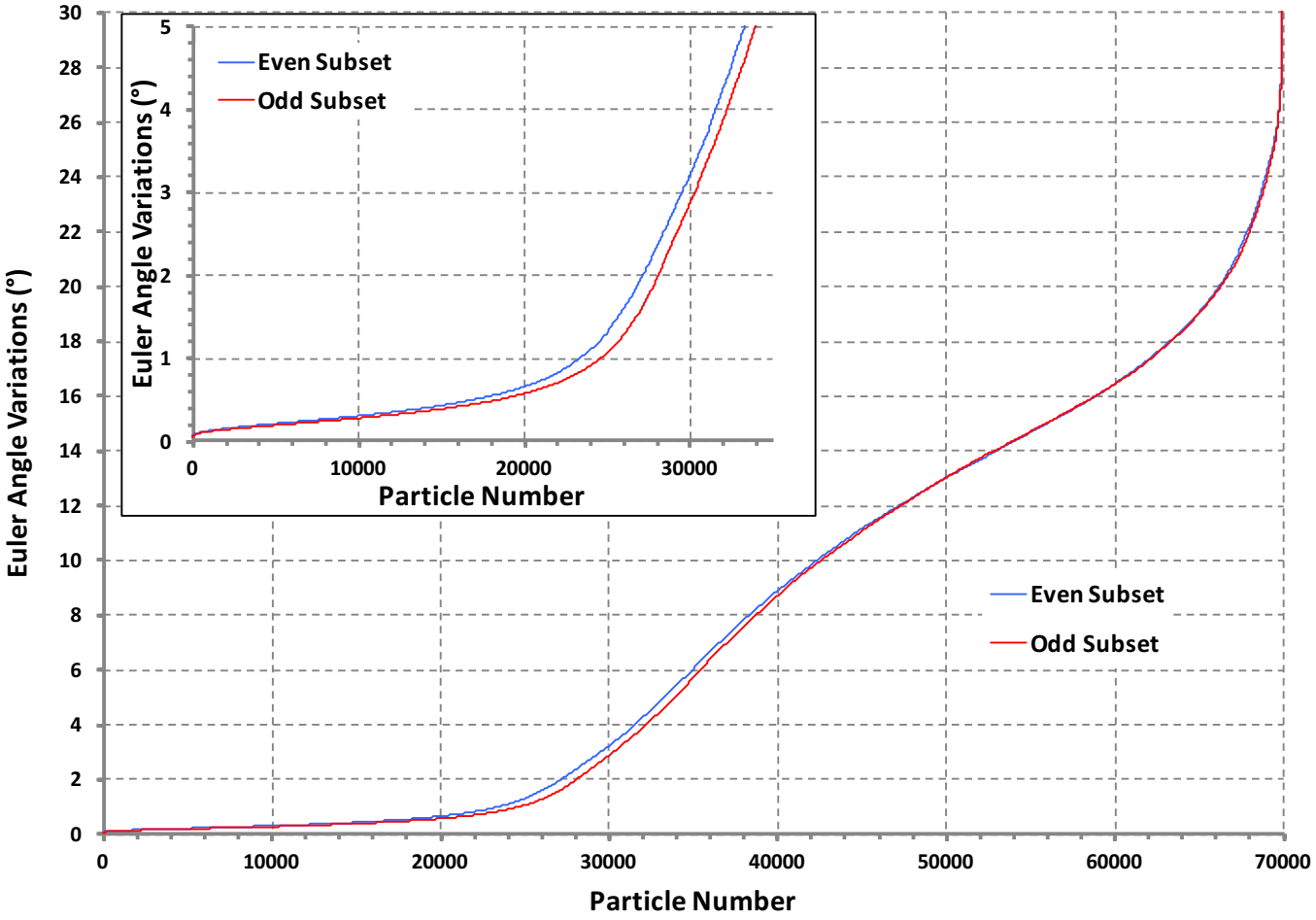

Figure S3. Related to Figure 2. Particle Euler angle variation plot. Three independent sets of Euler angles were determined by iterative refinements using 4x binned particles and independent *de novo* initial models. The variations among the three sets of Euler angles were sorted and plotted. The inset shows the zoomed region for the 35000 particles with smallest variations. Using 2° for Euler angle variations and 1 pixel for center variations (plot now shown) as the threshold, ~27k particles (~40% of all particles) were selected from the even and odd datasets for further refinements.

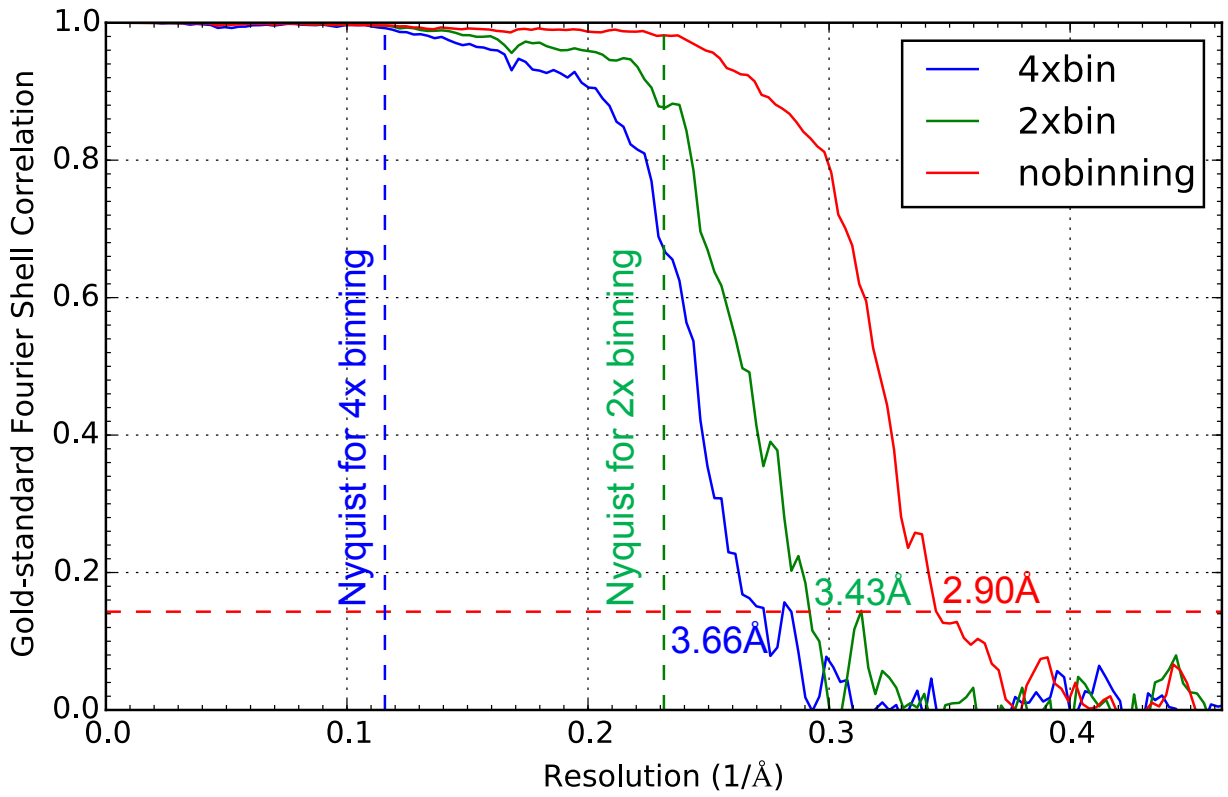

Figure S4. Related to Figure 2. FSC curves for reconstructions with particle parameters refined using images of different binning levels. The particle parameters of 4x and 2x binned images were transferred to particles without binning (*i.e.* adjusting center positions while reusing Euler angles). These particles parameters were directly used to reconstruct 3-D maps from particles without binning. FSC was then computed for the resultant two maps, one from even and one from odd dataset. The Nyquist resolution for 4x and 2x binned images were indicated by the blue and green vertical dash lines, respectively.

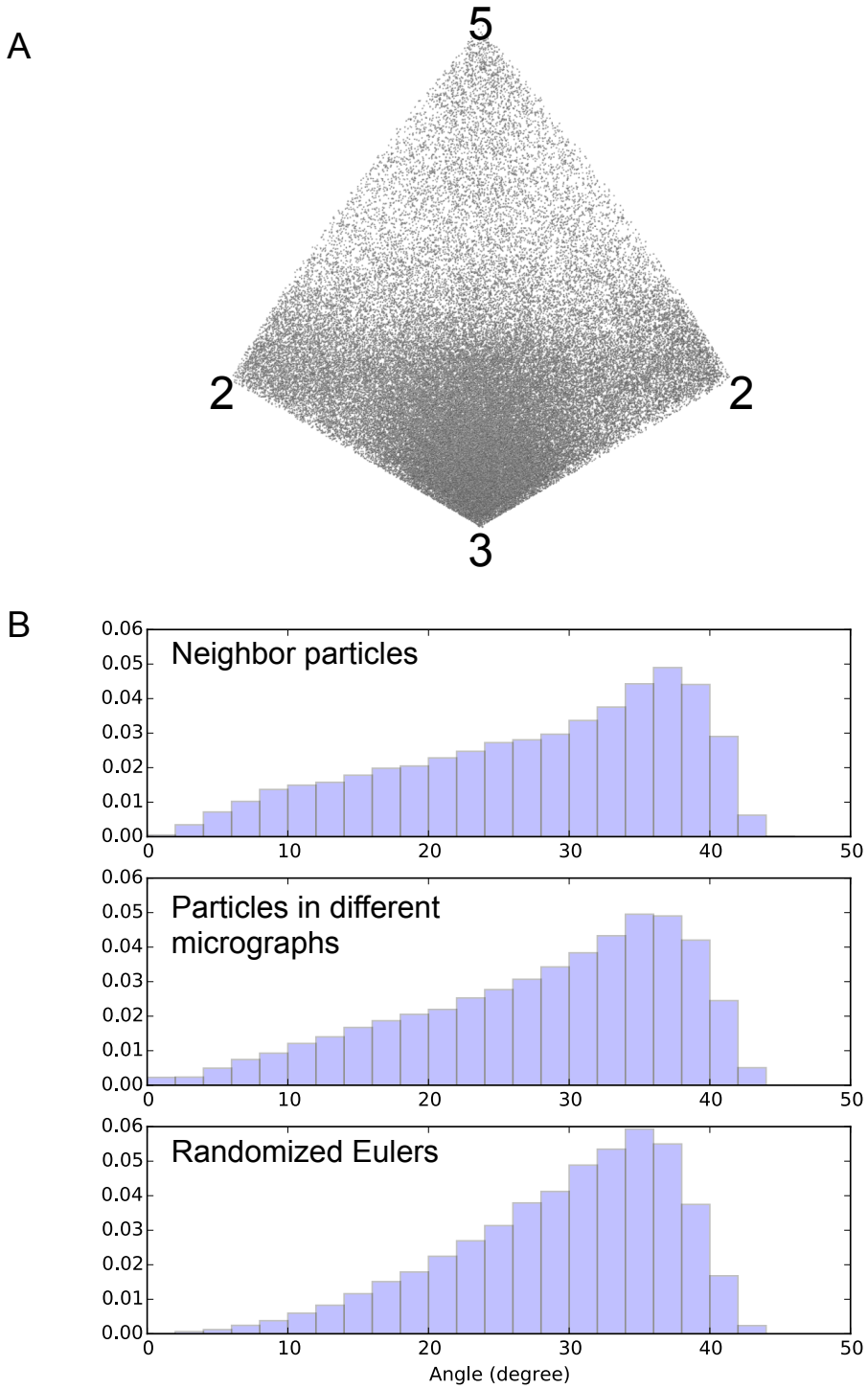

Figure S5. Particle view and inter-particle view distributions. Related to Figure 1. (A) Euler angle distribution in an icosahedral asymmetric unit. The distribution with more abundant views around icosahedral 3-fold axis relative to 5-fold axis is typical for icosahedral viruses with relatively flatter triangular faces and protruding 5-fold vertices. (B) Inter-particle angle distribution. The angle is calculated as the smallest relative angle among the 60 relative angles between a particle's Euler angle and the 60 icosahedral symmetry related Euler angles of the other particle. Neighbor particles (top panel) are computationally defined as the pairs of particles with their center-to-center distance no more than 1.25 of particle diameter (19 nm). The control distribution with randomized Euler angles (bottom panel) used uniform angle sampling on a unit sphere as specified in http://mathworld.wolfram.com/SpherePointPicking.html.

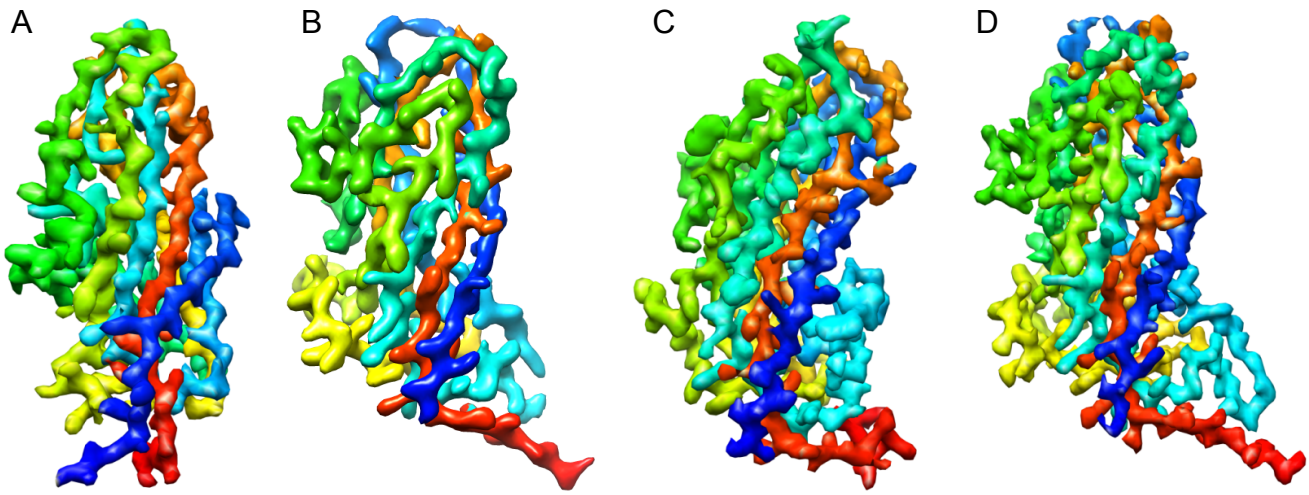

Figure S6. Related to Figure 5. Comparison of cryo-EM and X-ray crystallographic density maps. Shown are X-ray 2Fo-Fc density maps of three viral proteins at (A) 3.02 Å resolution (PDB ID: 2YGC, vaccinia virus d13 protein), (C) 2.90 Å resolution (PDB ID: 2IZW, ryegrass mottle virus), and (D) 2.35 Å resolution (PDB ID: 3R0R, PCV2 consensus sequence). Our 2.9 Å resolution cryo-EM map of PCV2 (Yamagata strain) is shown in (B). The density maps are rainbow colored from blue (N-terminus) to red (C-terminus). The electron densities of the three crystal structures were downloaded from the Electron Density Server (http://eds.bmc.uu.se/eds).

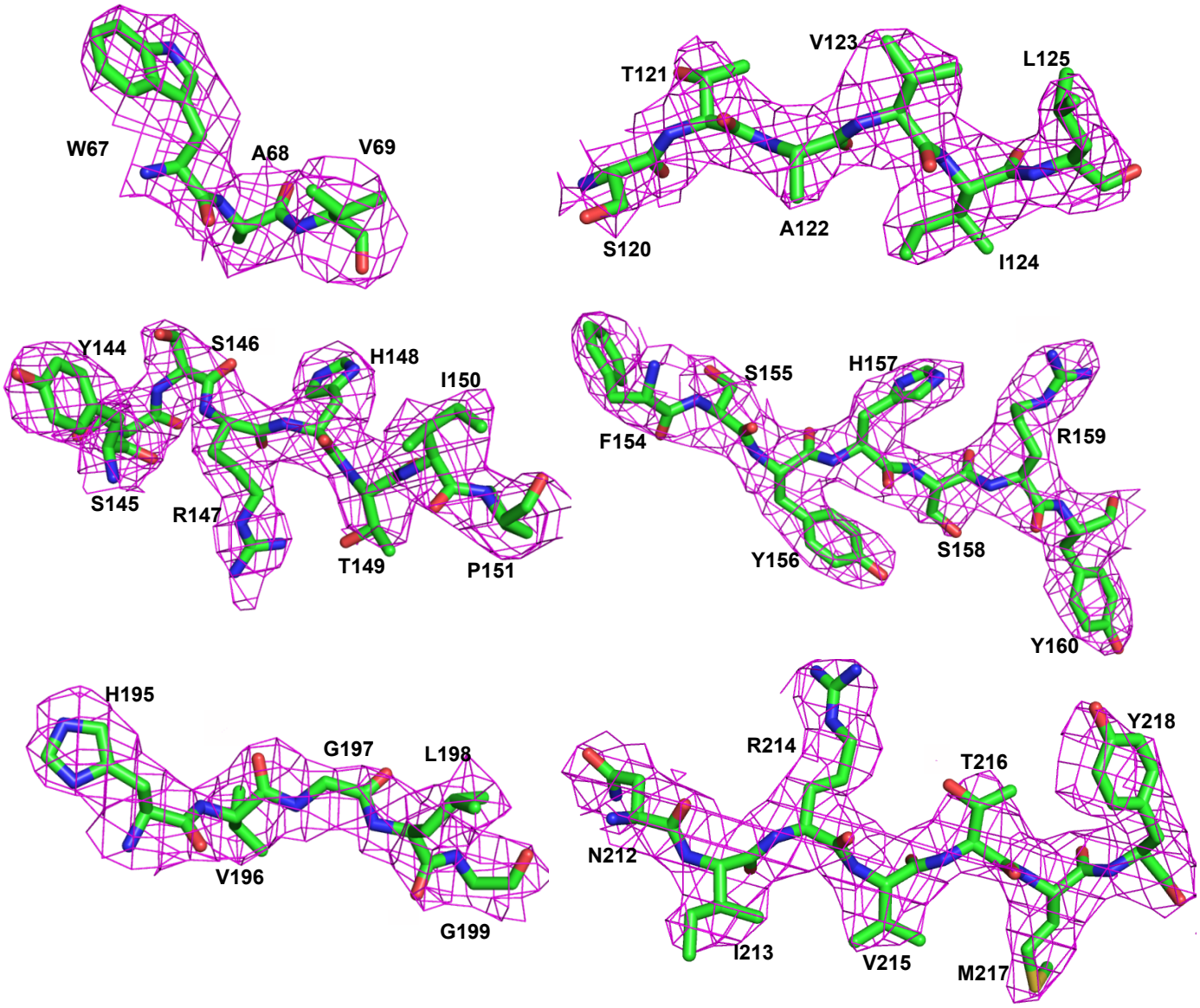

Figure S7. Related to Figure 5. Cryo-EM map densities superimposed with PCV2 atomic model. The electron densities are shown as magenta mesh and the atomic model is shown as green, blue, and red sticks. The density segments are sampled throughout the polypeptide chain to present the overall quality of the map.

Figure S8. Related to Figures 6 and 7. Sequence alignment of the Yamagata strain (this work) and the consensus strain used in the crystal structure (PDB ID: 3R0R). The residues colored in magenta are different in these two strains. The secondary structures are shown below the sequences with α-helices in yellow tubes, β-strands in green arrows, loops in blue lines, and unresolved regions in blue dotted lines. The 8 β-strands (BIDG and CHEF) for the jelly-roll β-barrel are labeled in red following conventional naming scheme.